ARTICLE

Eliminating genes for a two-component system increases PHB productivity in *Cupriavidus basilensis* 4G11 under PHB suppressing, nonstress conditions

Kyle Sander[1,2] | Anthony J. Abel[1,3] | Skyler Friedline[1,2] | William Sharpless[1] | Jeffrey Skerker[1,2,4] | Adam Deutschbauer[4] | Douglas S. Clark[1,3] | Adam P. Arkin[1,2,4]

[1]Center for the Utilization of Biological Engineering in Space, Berkeley, California, USA

[2]Department of Bioengineering, University of California, Berkeley, California, USA

[3]Department of Chemical & Biomolecular Engineering, University of California, Berkeley, California, USA

[4]Environmental Genomics and Systems Biology Division, Lawrence Berkeley National Laboratory, Berkeley, California, USA

Correspondence
Adam P. Arkin, Innovative Genomics Institute, 2151 Berkeley Way, Berkeley, CA 94074, USA.
Email: APArkin@lbl.gov

Present addresses
Skyler Friedline, Genome Science and Technology Graduate Program, University of British Columbia, Vancouver, British Columbia, Canada.

William Sharpless, Department of Bioengineering, University of San Diego, San Diego, California, USA.

Jeffrey Skerker, Ginkgo Bioworks, Emeryville, California, USA.

Funding information
National Aeronautics and Space Administration, Grant/Award Number: NNX17AJ31G

Abstract

Species of bacteria from the genus *Cupriavidus* are known, in part, for their ability to produce high amounts of poly-hydroxybutyrate (PHB) making them attractive candidates for bioplastic production. The native synthesis of PHB occurs during periods of metabolic stress, and the process regulating the initiation of PHB accumulation in these organisms is not fully understood. Screening an RB-TnSeq transposon library of *Cupriavidus basilensis* 4G11 allowed us to identify two genes of an apparent, uncharacterized two-component system, which when omitted from the genome enable increased PHB productivity in balanced, nonstress growth conditions. We observe average increases in PHB productivity of 56% and 41% relative to the wildtype parent strain upon deleting each gene individually from the genome. The increased PHB phenotype disappears, however, in nitrogen-free unbalanced growth conditions suggesting the phenotype is specific to fast-growing, replete, nonstress growth. Bioproduction modeling suggests this phenotype could be due to a decreased reliance on metabolic stress induced by nitrogen limitation to initiate PHB production in the mutant strains. Due to uncertainty in the two-component system's input signal and regulon, the mechanism by which these genes impart this phenotype remains unclear. Such strains may allow for the use of single-stage, continuous bioreactor systems, which are far simpler than many PHB bioproduction schemes used previously, given a similar product yield to batch systems in such a configuration. Bioproductivity modeling suggests that omitting this regulation in the cells may increase PHB productivity up to 24% relative to the wildtype organism when using single-stage continuous systems. This work expands our understanding of the regulation of PHB accumulation in *Cupriavidus*, in particular the initiation of this process upon transition into unbalanced growth regimes.

KEYWORDS
bioplastic, *Cupriavidus*, histidine kinase, PHB, RB-TnSeq

1 | INTRODUCTION

Bioderived plastics offer a potentially sustainable and renewable alternative to conventional petroleum-derived plastics. Widespread production and use of bioproduced plastics remain limited, in part, by low productivies (Bellini et al., 2022; Kachrimanidou et al., 2021; Pavan et al., 2019). Species of the bacterial genus *Cupriavidus* exhibit the highest productivities of natural or recombinant poly-hydroxybutyrate (PHB) producing organisms (Choi et al., 2020). While it is possible to attain very high PHB productivities using a variety of organisms through sophisticated multistage bioreactor or feeding regimes (Atlić et al., 2011; Kim et al., 1994; Vlaeminck et al., 2022), these systems can require very high substrate loadings, and necessitate regular shutdown and start-up cycles in-between batches (Choi et al., 2020; Franz et al., 2011; Kim et al., 1994; Lee & Chang, 1993). Maintaining high substrate utilization remains important for both economically viable industrial bioplastic production (Pavan et al., 2019) and in resource-constrained, remote, and austere bioplastic production and deployment settings (Berliner et al., 2021).

PHB is natively produced in *Cupriavidus* during conditions when the organism is incurring any of a variety of metabolic stresses, and the productivity potential in *Cupriavidus* is typically maximized by initiating high PHB productivity via one or several of these stresses after a period of cell biomass production. This strategy typically requires multistage sophisticated bioprocesses (Koller & Braunegg, 2015; Vadlja et al., 2016). These processes typically require between two and five sequential batch or fed-batch growth/incubation steps (Atlić et al., 2011; Cavalheiro et al., 2009). Additional steps are necessary because of the apparently regulated nature of PHB production in these organisms. This regulation necessitates augmenting the extracellular environment ultimately to metabolically stress the organisms after an initial period of high cell growth. It is during these subsequent discrete stages of the process where most of the PHB is accumulated. Fed-batch systems are also often necessary to avoid high initial concentrations of substrate which may be metabolically toxic to the organisms (Vlaeminck et al., 2022).

Though relatively high PHB productivities have been achieved, intracellular PHB accumulation during nonstressed, balanced growth remains low; ~<50% PHB cdw (cell dry weight) and thus there remains further potential to increase PHB accumulation in the organism under fast-growing, replete conditions.

We propose overall productivity might be increased further by engineering *Cupriavidus* to produce higher amounts of PHB continuously, during periods of balanced growth. Organisms that produce PHB using recombinant genes to produce PHB do so in an apparently constitutive manner (Ahn et al., 2000). One of the highest productivities (g PHB/L/h) achieved in *Cupriavidus* was achieved by allowing a slight amount of residual growth, while still maintaining nutrient-limited conditions (Grousseau et al., 2014), suggesting that growth-associated PHB production is not only possible but is a promising way to rapidly increase overall PHB productivity. Similarly, elemental mode analysis suggests the possibility and promise of constitutive PHB bioproduction by *Cupriavidus* (Islam Mozumder et al., 2015).

Only segments of the genetic and metabolic mechanisms regulating PHB production in *Cupriavidus* have been elucidated, and engineering genes of the PHB production pathway (*phaCAB*) directly has yet to enable growth-associated PHB production in *Cupriavidus*. This suggests its productivity is regulated by the availability of redox cofactors (Grousseau et al., 2014) and/or determined by regulatory elements (Cai et al., 2015; Juengert et al., 2017, 2018).

Enforcing growth-associated bioproduction has been a strategy for increasing productivity for a number of products and host/chassis organisms (Klamt & Mahadevan, 2015) and for PHB productivity in *Synechosystis* (Testa et al., 2022). This generic strategy considers only the augmentation of metabolic genes and often requires tenuous and unreliable manipulation of many genes in a single strain. This analysis can also indicate that growth-coupled production of a particular product is simply not possible given the metabolic systems considered. Alternatively, eliminating native regulatory genes from the genome has been shown to increase PHB productivity in *Cupriavidus* during conditions of minimized oxygen stress (Tang et al., 2022).

In this work, we aim to genetically engineer PHB-producing *Cupriavidus basilensis* 4G11, for constitutive bioproduction of PHB. The multiply regulated nature of PHB synthesis (Cai et al., 2015; Juengert et al., 2017, 2018; Tang et al., 2022) suggests that an unbiased, mechanism agnostic, genome-wide search for genes regulating PHB productivity under nonnutrient restricted conditions could yield targets for engineering production under balanced growth. For this reason, we chose to screen an existing RB-TnSeq transposon library of *C. basilensis* 4G11 (Price et al., 2018) for mutants exhibiting constitutive bioproduction of PHB. *C. basilensis* 4G11 is closely related to the well-studied and industrially relevant PHB-producing strain *C. necator* H16; with 79.5% of *C. basilensis* 4G11 proteins having one or more homologs in *C. necator* H16 (Supporting Information: Figure S1). *C. basilensis* 4G11 was originally isolated from subsurface groundwater at the Field Research Center at Oak Ridge National Laboratory which contains legacy contaminants originating from the production of nuclear materials (Ray et al., 2015). We find that the wildtype organism produces similar amounts of PHB as the model PHB-producing organism *Cupriavidus necator* H16 (data not shown).

We adapted and used a fluorescence assisted cell sorting (FACS)-based screen for intracellular PHB which utilizes BODIPY 493/503 dye (Kacmar et al., 2006) (Figure 1), and developed a culture preconditioning protocol that significantly suppressed/eliminated PHB productivity (Supporting Information: Figure S2). PHB productivity in candidate mutants was then measured directly in these same conditions and shown to be higher, suggesting a role for these genes in regulating the onset of PHB production in *Cupriavidus*, and showing that the elimination of these genes may enable constitutive PHB bioproduction.
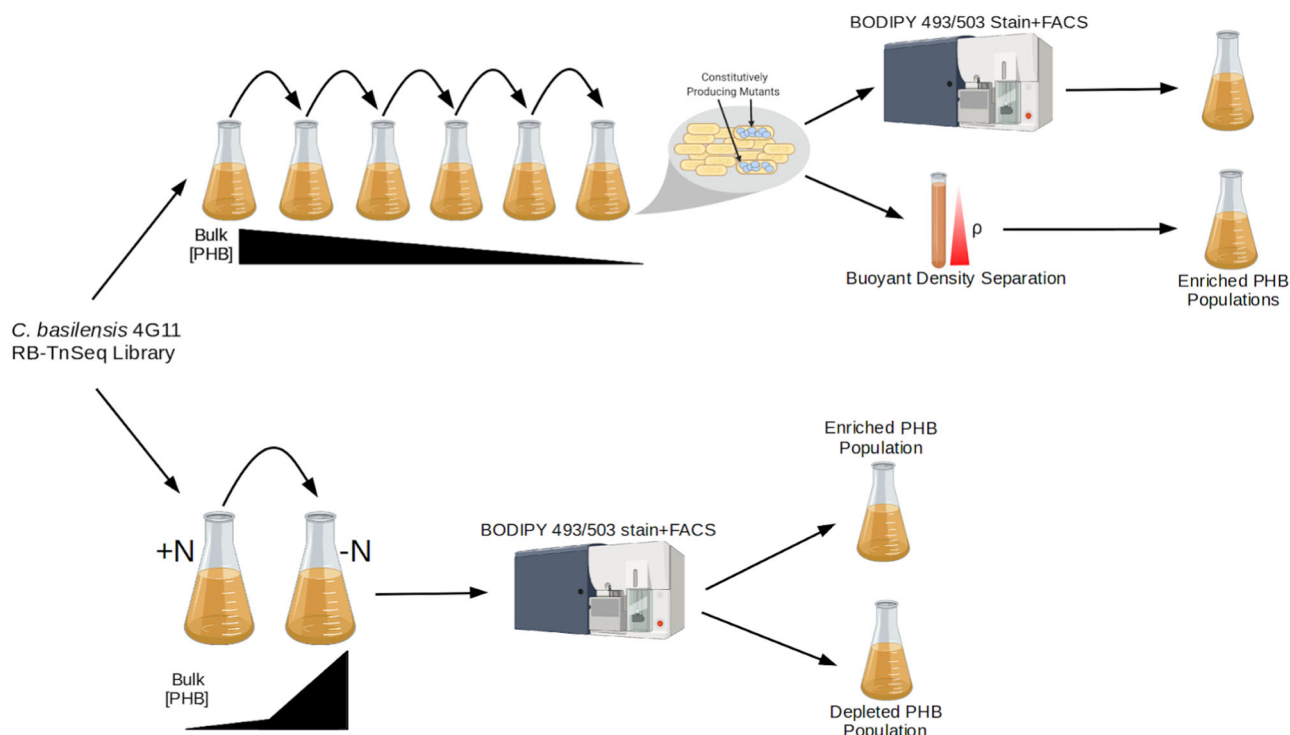
FIGURE 1 Dual screening strategy utilized in this study to isolate mutants exhibiting increased poly-hydroxybutyrate (PHB) accumulation phenotype from *Cupriavidus basilensis* 4G11 RB-TnSeq libraries. Cells are repeatedly subcultured in replete medium to maximally suppress PHB accumulation among the bulk population, shown along the top of the figure. From this population, high-PHB accumulating ("constitutively producing") mutants were selected using two different fractionation methods: FACS and buoyant density separation. Nitrogen-starved cultures were first grown in replete medium, followed by an incubation period in nitrogen-free medium in which the bulk population accumulates high amounts of PHB, shown along the bottom of the figure. From this population, we separately selected the highest and lowest accumulating PHB mutants. FACS, fluorescence assisted cell sorting.

2 | RESULTS

2.1 | Development of screen to suppress PHB production in the wildtype organism

In our screen, we sought mutants which accumulate differentially more PHB in nonstress, highly replete, fast-growing conditions; conditions in which wildtype species of *Cupriavidus* and other PHB accumulating organisms accumulate very little, if any, PHB. To assess this specific phenotype, we developed a method for culturing *C. basilensis* 4G11 which reliably suppressed intracellular PHB accumulation to a minimal amount. This method resulted in cells in culture that were in a fast-growing, nutrient-replete state, as we see from the reproducible near-complete suppression of intracellular PHB (Supporting Information: Figure S2). This was achieved through frequent passaging of cultures, maintaining minimal culture optical density (OD), maximizing nutrient concentrations, and maintaining saturated dissolved oxygen conditions. This method for suppressing intracellular PHB was used before both RB-TnSeq library screens as well as before and during quantification of PHB productivity in candidate mutants. In practice, this minimized potential background PHB, and served as a nonstressed, nutrient-replete state in which we performed PHB quantification in candidate mutants for constitutive PHB bioproduction.

2.2 | Screening RB-TnSeq libraries for high-producing mutants

We performed forward genetic screens on a pre-existing *C. basilensis* 4G11 RB-TnSeq library (Price et al., 2018) for increased PHB productivity under both PHB-suppressed replete conditions (as described in Section 2.1), and in conditions inducing high PHB accumulation; through incubation in a medium in which all nitrogen had been omitted after a period of initial cell growth in nitrogen-replete medium (Figure 1). We identified eight candidate genes whose transposon insertion mutant strains showed increased enrichment when screened for increased intracellular PHB in either replete, fast-growing conditions, or nitrogen-starved conditions (Supporting Information: Table S1). Several genes identified were genomically colocalized, suggesting possible interoperonic expression and/or related metabolic function; specifically RR42_RS17055 and RR42_RS17060 form two genes of an apparent two-component histidine kinase/response regulator system, while RR42_RS18960-RR42_RS18970 are genes involved in membrane asymmetry maintenance. The identified collocated genes also exhibited consistent gene fitness (Supporting Information: Figure S3) in several previously conducted stress exposure or defined nutrient auxotrophy assays (Price et al., 2018)

further implicating their related and/or dependent gene function (Price et al., 2021).

2.3 | Assaying candidate mutants for constitutive PHB productivity

We generated markerless whole-gene deletion mutants for identified genes to quantify their PHB productivity. We utilized genetic and conjugation methods developed previously for *C. necator* H16 (Juengert et al., 2018). Similar to *C. necator*, *C. basilensis* 4G11 was found to be gentamicin resistant (data not shown). For this reason, to make deletion mutants we utilized suicide vectors based on the pMQ30 backbone (Shanks et al., 2006) containing a kanamycin resistance marker in place of the gentamycin resistance marker on the original pMQ30 plasmid. We removed the heterologous kanamycin resistance using the *sacB* gene and sucrose counterselection. These mutants constitute, to our knowledge, the first markerless deletion mutants in this species.

We assayed these mutants for PHB productivity under fast-growing replete conditions. We found two mutants that consistently accumulated high amounts of PHB (Figure 2, Supporting Information: Figure S7) in this balanced-growth condition; a deletion mutant of the gene RR42_RS17060 which exhibited an average 56% higher PHB productivity relative to the wildtype parent strain, and a deletion mutant of the neighboring gene RR42_RS17055 which exhibited an average 41% higher PHB productivity relative to the wildtype parent strain. While mutants in other genes exhibited increased PHB productivity in single subcultures, no other genes assayed exhibited consistent productivity increase across subsequent subcultures as these two genes did.

This phenotype of mutants in these two genes appears to be specific to high-growth, nonstress, replete conditions. The PHB accumulation advantage disappears in ΔRR42_RS17055 and ΔRR42_RS17060 upon allowing replete, defined medium growth/incubations to continue to stationary phase, and when the same cells are subsequently incubated in defined minimal medium containing no
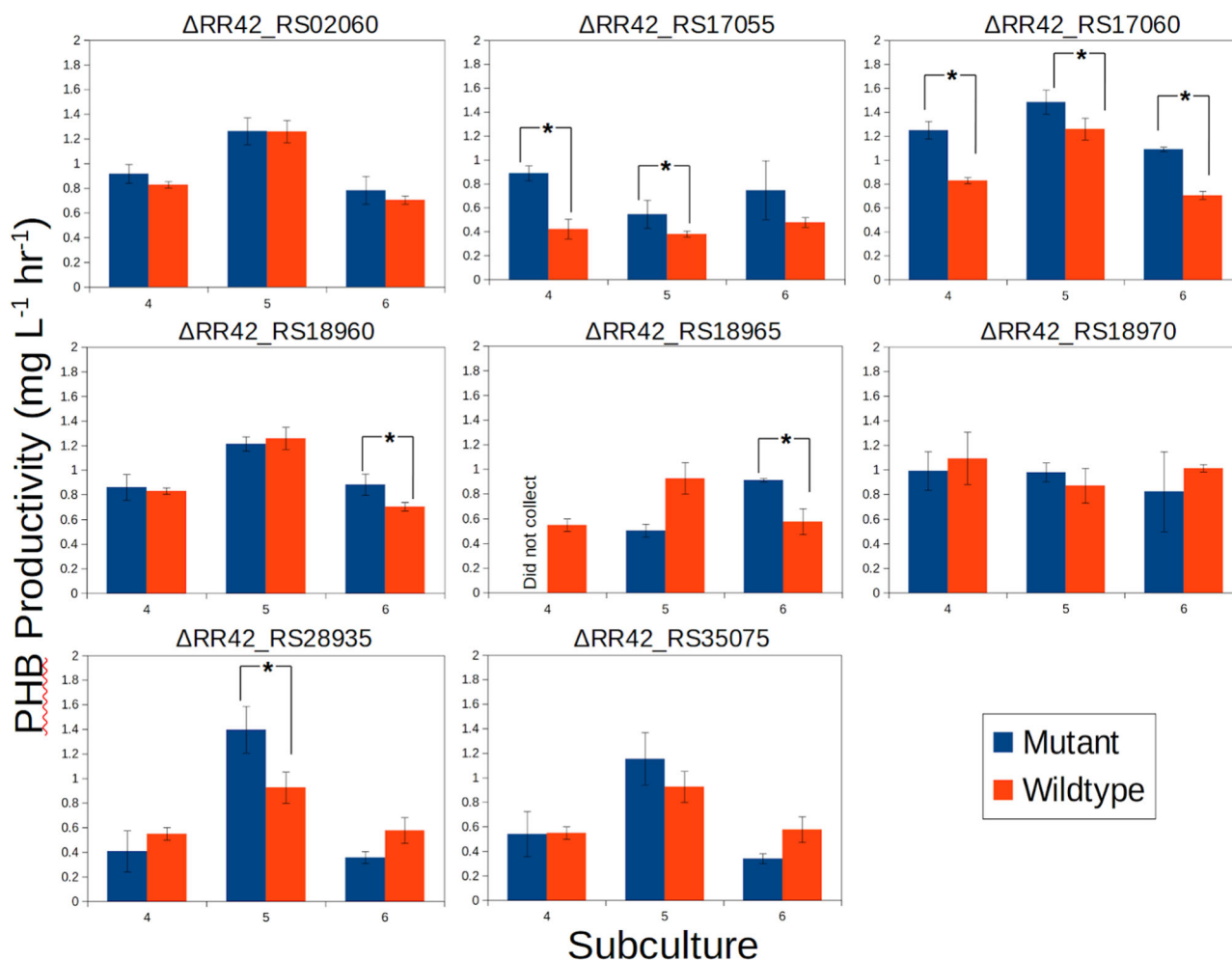
FIGURE 2 Accumulation of PHB in deletion mutants of selected genes during fourth to sixth subcultures in balanced-growth conditions. Genes encoding an apparent uncharacterized two-component system (RR42_RS17055-17060) consistently accumulate more PHB than the wildtype parent strain in nonstress conditions in which PHB accumulation is suppressed. * Denotes statistical significance (one tailed *t* test, *n* = 3, equal variance, *p* < 0.05). PHB, poly-hydroxybutyrate.

added source of nitrogen (Supporting Information: Figure S4). The wildtype organism accumulates more PHB than either mutant upon reaching the stationary phase after a 24 h growth period in replete, defined medium, and more than the ΔRR42_RS17060 mutant after a subsequent 24 h incubation in nitrogen-free, defined medium.

RR42_RS17060 is annotated as a hybrid histidine kinase and RR42_RS17055, annotated as a LuxR family transcription factor, is likely the cognate response regulator for the histidine kinase as it contains a response regulator domain within its coding region (Figure 3). Similar fitness patterns between these two genomically adjacent genes (Supporting Information: Figure S3) suggest they likely form a two-component signal sensing and transduction system (TCS). RR42_RS17055 also contains a DNA binding domain, suggesting it likely regulates the transcription of its target genes in response to signals sensed by the histidine kinase. The annotations of these two genes and those genes in the immediate genomic neighborhood do not suggest any information about the external stimulus that the system responds to, or the genes whose expression the system might be regulating. Promoter alignments of these two genes and the two additional genes which exhibit cofitness do not yield consensus sites indicative of potential operator sequences (data not shown).

2.4 | Productivity modeling indicates TCS mutants may increase PHB productivity

We built and interrogated a PHB kinetic model for two purposes: to confirm our hypothesis that this increase in PHB could be due to a decrease in reliance on unbalanced growth for the initiation of PHB production, and to decipher potential increases in PHB productivity that might be realized using these strains.

We adapted a PHB production model developed previously (Islam Mozumder et al., 2015) which has been utilized to model PHB production dynamics in *C. basilensis* 4G11 (Cestellos-Blanco et al., 2021). This kinetic model considers cell biomass growth, production of PHB, consumption, and cell growth inhibition of key metabolites acetate and nitrogen (in the form of ammonium chloride). It models the coupling of nitrogen concentration and PHB productivity through the key model parameter K_{PIN}, which represents the sensitivity and reliance of PHB accumulation to the nitrogen concentration for both wildtype and mutant strains. Our model fit for this parameter (see below) of the wildtype parent strain was nearly the same as predicted in a previous study utilizing the same growth medium through different culturing conditions (Cestellos-Blanco et al., 2021). We further recapitulated similar cell and PHB substrate yield values to known, previously calculated values (Supporting Information: Table S2).

In fitting the K_{PIN} parameter to our cell growth and PHB production data from single deletion mutants of the RR42_RS17055-17060 two-component system, we found this parameter to be much higher in these mutant strains than it was in the wildtype (Supporting Information: Table S2). This larger value of the parameter might be interpreted as our mutants' decreased reliance on nitrogen limitation metabolic stresses to initiate PHB accumulation. While our adaptation of this model assumes PHB accumulation is only coupled to nitrogen concentration, it is known that many metabolic stresses and nutrient deficiencies can initiate PHB production in the closely related *C. necator* (Islam Mozumder et al., 2015), and this may also be the case for *C. basilensis* 4G11 as well. The higher value of K_{PIN}
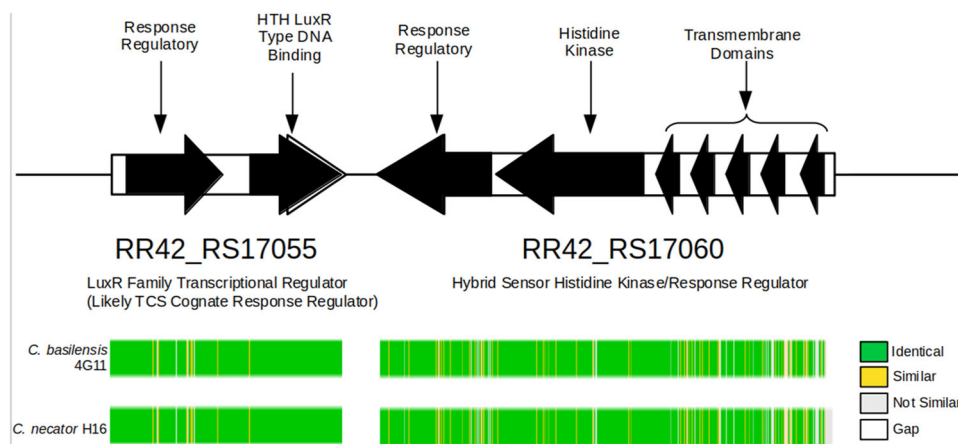
FIGURE 3 Genomic region, gene, and domain orientation of the two adjacent genes comprising the two-component system in *Cupriavidus basilensis* 4G11. RR42_RS17060 is annotated as a hybrid histidine kinase due to the presence of both histidine kinase domains and a response regulatory domain. RR42_RS17055 also contains a response regulatory domain as well as a DNA binding domain. Gene fitness similarities between the two genes (shown in Supporting Information: Figure S3) suggest they transduce the same signal(s) and the expressed proteins interact with each other. The presence of a DNA binding domain in RR42_RS17055 suggests signal transduction results in changes in DNA transcription. Colored bars indicate reciprocal amino acid homology between proteins encoded by these genes and their corresponding homologs encoded in the genome of *Cupriavidus necator* H16. Whole protein homology between the two organisms is 95% and 84% for the LuxR Family Transcriptional Regulator and Hybrid Sensor Histidine Kinase/Response Regulator, respectively.
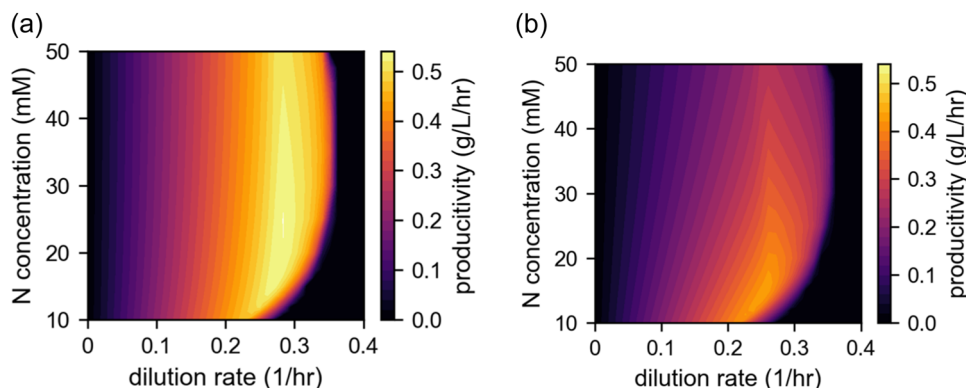
FIGURE 4 Volumetric poly-hydroxybutyrate productivity of (a) ΔRR42_RS17060 mutant and (b) wildtype *Cupriavidus basilensis* 4G11 in a simulated single-stage continuous system.

suggests that the two single deletion mutants (RR42_RS17055, RR42_RS17060) have PHB production metabolisms that are less coupled to nitrogen limitation or, perhaps more generally, to metabolic stress or nutrient deficiency, though this remains to be further explored or demonstrated.

We next developed a continuous bioproduction model to ascertain relevant and realistic bioproduction increases that might be realized by our single-strain deletion mutants. We modeled PHB productivity of the wildtype strain and the ΔRR42_RS17060 using key model parameters carried forward from the previous analysis. We modeled PHB production in a single-stage continuous system as this system has the distinct advantage of being simpler in configuration and operation than many of the more sophisticated multistage systems required to achieve high PHB productivity (when product yield and substrate conversion efficiency are similar to batch systems) in native nongrowth-associated wildtype *C. necator* (Atlić et al., 2011; Koller & Braunegg, 2015). In our simulated continuous system, the mutant is capable of 24% higher PHB productivity, generating a maximum of 0.541 g/L/h in optimized conditions (Figure 4a), compared to 0.437 g/L/h produced by the wildtype *C. basilensis* 4G11 (Figure 4b) in optimized conditions. Maximum mutant PHB productivity also exceeds wildtype productivities modeled over a range of dilution rates for both single and two-stage continuous systems (Supporting Information: Figure S5). Also, we observe an increase in the range of dilution rates and feed ammonia concentrations that would allow for near-optimal PHB productivity, relative to the wildtype organism.

3 | DISCUSSION

In this work, we use a forward genetic screen alongside a novel replete-condition PHB productivity assay to identify two genes whose omission from the genome results in increased PHB productivity under nonstress conditions, relative to the wildtype parent strain. These increases in productivity may translate to benefits in larger bioproduction settings given the possible use of simpler reactor configurations and operating needs relative to other multistage, batch configurations investigated previously. Also, an apparent decrease in necessary reliance on metabolic stress may simplify operational burden of far simpler reactor systems such as single-stage continuous systems.

Pathway and enzyme engineering for increased PHB synthesis and productivity in natively PHB-producing organisms typically retains the metabolic stress dependence of this process in these organisms and limits PHB productivity (Grousseau et al., 2014; Schmidt et al., 2016). This limitation unfortunately cannot be overcome by process optimization because of the inherent tradeoff between the cell-biomass-limiting effect of limiting a nutrient, and the need to limit such a nutrient to invoke the production of high amounts of PHB. PHB productivity increases realized through minimizing this stress dependence have been demonstrated (Tang et al., 2022) and removing the stress dependence for PHB production and enabling growth-associated PHB production has primarily taken two forms: engineering and exploration of the PHB synthesis/regulation in organisms that produce PHB natively (Mitra et al., 2022; Velázquez-Sánchez et al., 2020) and engineering the recombinant production of PHB (Horng et al., 2010; Theodorou et al., 2012) in organisms that do not natively produce PHB. In the former, achieving maximal PHB titers requires invoking a nutrient limitation or stress on the culture (Al Rowaihi et al., 2018; Alsiyabi et al., 2021; Wang & Lee, 1997). In the latter, PHB production is ostensibly not genomically regulated and can proceed in a growth-associated fashion. High PHB productivities have been achieved in both natively PHB-producing (Wang & Lee, 1997) (5.13 g/L/h, *Alcaligenes latus*), and recombinantly producing (Choi et al., 1998) organisms (4.63 g/L/h, recombinant *Escherichia coli*). High PHB production in organisms that natively produce PHB typically involves two phases; an unproductive phase of nutrient-replete driven cell growth (where little to no PHB is produced) followed by a nutrient-depleted phase of PHB productivity. Unlike the natively producing organisms, recombinantly producing organisms are capable of producing PHB during the entirety of a bioproduction batch cycle. Even with this unproductive period in native PHB producers, the highest demonstrated productivities in a

typical batch cycle of native and recombinant producers is roughly equivalent. Eliminating stress dependence in natively PHB-producing organisms would allow for PHB production during this otherwise unproductive initial phase and stands to greatly increase overall PHB productivity in these organisms. The mutations identified, constructed, and assayed in this work enable this potential productivity increase as they decrease dependence on stress for producing PHB in natively producing organisms, and do so without impacting PHB productivity in the nutrient-depleted phase of production.

Maintaining high product yield (g PHB/g substrate) and intracellular PHB content (% cdw) are also critical to cost-effective industrial bioplastic production (Choi & Lee, 1999; Van Wegen et al., 1998). Particular application scenarios require that high product yield must be maintained, mainly when substrate costs are high and in remote and austere environments such as long-term missions in space where access to feedstock material might be limited (Berliner et al., 2021). Both native (Wang & Lee, 1997) (A. latus, 0.99 g PHB/g carbon, 88% cdw) and recombinant (E. coli, 0.975 g PHB/g carbon (Napathorn et al., 2021), 73% cdw (Choi et al., 1998) PHB producers have exhibited comparably high values of these metrics and there is no apparent clear choice in host organism or strategy to achieve maximally high PHB productivity. Regardless of the strain employed for bioproduction, continuous fermentation can entail simpler reactor configurations, reduced downtime, and lower capital costs (Harrison et al., 2015; Konstantinov & Cooney, 2015; Yang et al., 2020). Improvements in either PHB productivity or efficiency will need to come from bioprocess or strain improvements. One way to improve these metrics would be to remove the productivity-limiting stress dependence in organisms that produce PHB natively. Little work has been done in continuous systems using native organisms and it is unclear what the productivity ceiling might be in this context, how far current demonstrated productivities are from this ceiling, and how much improvement may be engineered by way of strain or process improvement.

In addition to the findings herein, one other stress-dependent regulator of PHB synthesis has been shown to impart growth-associated PHB production. Overexpression of rpoN increased PHB productivity 77.5% and 103.1% when cultured in an O_2-sparged nonstress condition (Tang et al., 2022). We find no evidence to suggest this regulatory scheme may overlap with that of the two-component system identified in this work. This suggests that these two regulatory mutations may be combined in a single strain and plausibly further reduce the stress dependence of PHB production in species of C. necator.

An important but often overlooked consideration is that batch PHB and bioplastic productivities are typically calculated only during productive periods of cell culture. These calculations do not account for the full duration of an individual batch reactor cycle which include shutdown/startup processes such as clean-in-place, sterilized-in-place, seed inoculation preparation (Krauβe, 2009), auxiliary equipment equilibration, calibration, reactor loading, as well as washing, elution, and regeneration of downstream purification processes (Harrison et al., 2015)—all of which may be nonproductive periods

of time in between batches but are nonetheless necessary parts of batch operation. Operating multiple batch reactors with sophisticated overlapping batch scheduling, and product holding capacity can work to minimize these intermediary nonproductive periods, but requires more equipment and thus higher capital cost (Choi & Lee, 1999; Van Wegen et al., 1998). When accounting for these various nonproductive fermentation downtimes in batch processes, comparative productivities have been shown to be as much as two-fold higher in continuous systems producing other bioproducts (Bailey & Tähtiharju, 2003), though process and control complexity inherent to continuous bioproduction and regulatory burdens have largely prevented widespread adoption (Fisher et al., 2019; Konstantinov & Cooney, 2015).

The maximum productivity modeled in this work (0.541 g/L/h), while lower or similar to values demonstrated in batch systems mentioned above, is a proof-of-concept demonstrations using unoptimized genetic mutants modeled in what are likely continuous growth conditions which can be greatly improved upon. In this work, we also empirically fit a product yield of 1.27 g PHB/g carbon (Supporting Information: Table S2), which exceeds those of commercial and batch systems which predominantly use hexoses as substrates (Choi & Lee, 1999; Wang & Lee, 1997). Stacking of beneficial mutations and optimizing continuous bioproduction may increase observed productivities to the level achieved previously, and further increase product yield, all while leveraging the reduced downtime and simpler reactor configurations of reduced size that continuous bioproduction can offer (Konstantinov & Cooney, 2015).

Methods for continuous, constitutive production of PHB in Cupriavidus have been proposed and sought previously (Koller & Braunegg, 2015), though none (to our knowledge) have utilized strains that minimize stress-dependence of PHB synthesis. In one instance, PhaB was engineered to be NADH-dependent to couple with a recombinant NADH-dependent glucose-6-phosphate to provide needed NADH-reducing power (Olavarria et al., 2022) and allow for fermentative, anaerobic PHB production without the need to inhibit biomass formation. However, this strategy was not fully demonstrated, and may still be subject to gene regulatory constraints not considered. Many other metabolic systems previously shown to impact PHB accumulation in species of Cupriavidus were regulatory systems. These include phosphoregulation (Juengert et al., 2018; Krauβe, 2009), the PhaR protein that binds upstream of and transcriptionally regulates the phaCAB operon (Cai et al., 2015; York et al., 2002), PHB granule associated phasins (Pötter et al., 2005; Tang et al., 2022; York et al., 2002), and the stringent response (Juengert et al., 2017; Karstens et al., 2014). The accumulation of PHB in Cupriavidus thus appears to be regulated in multiple ways and a comprehensive understanding of its regulation remains unknown, including any regulators which may sit atop known regulatory machinery in a hierarchy. In this work, we found another regulatory element capable of impacting PHB productivity, though the full scope of its regulatory sensing and action remains unknown. Knowing the regulon and metabolite(s) it responds to may allow for a more comprehensive understanding of the regulation of PHB synthesis in

this and other organisms. Such knowledge may also suggest more effective methods with which to engineer increased PHB productivity, through deregulating the onset of PHB synthesis, in this and related organisms.

The two genes identified in this screen demonstrated to increase balanced-growth productivity are not functionally characterized. They likely comprise a two-component system responsible for sensing a metabolic signal and transducing a response signal through altering gene transcription, and the two genes are colocated adjacent to each other on the genome (Figure 3). RR42_RS17060 is annotated as a hybrid histidine kinase and contains domains associated with both histidine kinase activity and a response receiver/regulator in the same coding DNA sequence. The adjacent gene RR42_RS17055 also contains a response regulator domain, as well as an helix-turn-helix DNA binding motif. A similar phenotype of knockout mutants of these genes suggests they are part of the same signal cascade. Additionally, the increased PHB accumulation phenotype exhibited by these two mutants is apparently specific to fast-growing, nonstress conditions. The disappearance of the increased PHB accumulation phenotype (Supporting Information: Figure S4) in more limiting and stress conditions suggests that the regulatory differences invoked by the two-component system may be specific to the early onset of PHB accumulation in the organism and may be yet another part of the complex regulation of PHB accumulation in this and other species of *Cupriavidus*.

Two other genes share similar fitness phenotypes with these genes (Supporting Information: Figure S3) in an array of other assays performed previously (Tang et al., 2022), though annotations of these genes do not readily indicate the cellular function this apparent system may be directly regulating, nor how this regulation may be otherwise impacting PHB accumulation in replete, high growth-rate conditions. Cofitness analysis, made possible by another study using this same RB-TnSeq library (Price et al., 2018), indicates two other genes which show consistent fitness patterns with genes comprising this apparent two-component system (Supporting Information: Figure S3). One gene is annotated as a Serine/ Threonine Protein Phosphatase; RR42_RS04895. While the specific function or signal of the protein encoded by this gene remains unknown, this class of protein is known to participate in phosphoregulation, through protein dephosphorylation activity, of stress-related signal cascades (Shi, 2009). Similarly, the interaction partners or specific function of RR42_RS02045, annotated as a GTPase remain unknown. Protein sequence homologs exhibiting >84% homology to all four proteins (the two collocated apparent TCS genes, Ser/Thr Protein Phosphatase, and GTPase) also exist in the genome of the well-studied closely related notable PHB producer *C. necator* H16, suggesting these genes may also play a role in regulating the onset of PHB production in this organism as well.

Previously it was demonstrated that CrbR (part of the CrbR/CrbS two-component system) regulates the expression of genes involved in acetyl-coenzyme A (CoA) metabolism in *Pseudomonas fluorescens* (Sepulveda & Lupas, 2017), and the LuxR family transcription factor encoded by RR42_RS17055 is 34% homologous to CrbR in *P. fluorescens*. We find putative operator sites upstream of the *acs* (acetyl-CoA

synthetase) gene, a gene in the CrbR regulon of *P. fluorescens*, across diverse species of *Cupriavidus* (Supporting Information: Figure S6). However, the same sites cannot be identified upstream of either RR42_RS17055 or RR42_RS17060. Furthermore, there is low whole-protein sequence homology between RR42_RS17060 and CrbS of *P. fluorescens*, further suggesting the two systems are not homologous.

RR42_RS17055-17060 also exhibit protein homology to VsrB and VsrC (60.1% and 62.1% identity, respectively) of *Ralstonia solanacaerum* ATCC 11696 across > 97% of the length of the protein-coding sequences. VsrBC is a two-component hybrid histidine kinase just as RR42_RS17060 and RR42_RS17055 is predicted to be. These proteins also share strong domain and positional homology (data not shown) to the TCS genes identified in this study. The VsrBC two-component system has been shown to regulate exopolysaccharide (EPS) I exopolysaccharide biosynthesis through regulating expression of genes of the EPS I gene cluster in *R. solanacaerum* AW (Garg et al., 2000; Mori et al., 2018; Schell, 2000) and EPS I-derived exopoly-saccharides have been shown to be the primary mechanism enabling plant virulence activity in the organism. It is not known whether *C. basilensis* 4G11 can colonize plant tissue, though other closely related species of *Cupriavidus* are known to do so (Barrett & Parker, 2006; Lykidis et al., 2010). VsrC binds a particular operator site with the consensus sequence GCGGGGGAA upstream of the EPS I biosynthesis gene cluster in *R. solanacaerum* AW and, in conjunction with XpsR, activates expression of the EPS I locus (Garg et al., 2000; Mori et al., 2018). We were unable to identify this operator site in the homologous upstream region of the EPS I gene cluster in *C. basilensis* 4G11, or in other closely related species of *Cupriavidus*. Despite this, RR42_RS17055-17060 may be the VsrBC two-component system, perhaps binding at a different operator site sequence in *C. basilensis* 4G11 than that identified in *R. solanacaerum* AW, VsrBC is not known to directly regulate PHB accumulation in *Cupriavidus* or any other species of bacteria, to our knowledge. If these genes are responsible for activating EPS I, eliminating either of these genes may facilitate such a carbon metabolism flux redirection toward PHB biosynthesis, yielding the phenotypes we observe. Alternatively, RR42_RS17055-RS17060 may regulate both EPS I expression/biosynthesis and PHB accumulation simultaneously.

To date, no engineering or interrogation of two-component systems has been done in species of *Cupriavidus* for the purposes of increasing PHB production or deciphering TCS-related aspects of the native regulation of PHB synthesis/mobilization. However, two-component systems have been shown to regulate PHB synthesis in other bacteria. Overexpressing the native *E. coli* AtoSC two-component system activates fatty acid biosynthesis genes in an *E. coli* mutant expressing *C. necator* phaCAB genes and results in increased overall PHB titer and per-cell PHB accumulation (Theodorou et al., 2012), linking native fatty acid metabolism to heterologous PHB production in the organism. The globally regulating GacS/A two-component system's impact on PHA synthesis has been studied in various organisms. GacS knockouts in *Pseudomonas putida* and *Azotobacter vinelandii* exhibit decreased or wholly eliminated PHB production in *N*-starved conditions (Castañeda et al., 2000; Ryan et al., 2013). The GacS/A regulatory mechanism represses *phaR*

expression in *Pseudomonas chlororaphis* PA23 post-transcriptionally in conjunction with messenger RNA-binding protein RsmA (Hernandez-Eligio et al., 2012). Gene knockouts of the NtrBC two-component system regulating nitrogen assimilation display increased PHB production (Olaya-Abril et al., 2018) and suggest elevated NADPH/NADP+ ratios can drive PHA synthesis independent of C/N ratios in the growth environment (Sacomboio et al., 2017).

The successful leveraging of two-component system engineering for bioproduction increase, and the identification of a two-component system shown to impact PHB productivity in this study suggests these systems may be leveraged further in *Cupriavidus* to increase PHB productivity in both native and recombinantly producing organisms and to further elucidate the complex regulation of PHB productivity in these organisms (Rajeev et al., 2020). While further molecular regulatory and mechanistic information about this two-component system remains to be elucidated, utilizing these mutations to engineer bioproducing strains may allow for simpler, single-stage continuous bioreactor settings to produce PHA using bacterial hosts. Similarly, engineering this system may relieve the constraint of needing to invoke nitrogen limitation or other stress, and the reliance on complicated, multistage bioreactor systems necessary for this, allowing instead the use of simpler continuous systems to achieve similar or greater PHA productivities.

4 | CONCLUSION

We identify genes encoding a two-component system (RR42_RS17060; a hybrid histidine kinase and RR42_RS17055; a LuxR family transcription factor with a response regulator domain) capable of impacting PHB accumulation in *C. basilensis* 4G11. When each gene is individually omitted from the genome, these mutants are capable of producing higher amounts of PHB in balanced growth conditions (56% and 41% higher, respectively, for ΔRR42_RS17060 and ΔRR42_RS17055). The absence of this phenotype in unbalanced growth conditions suggests these genes may impart their impact early in the process of initiating PHB accumulation in the cells and are yet another regulatory element shown to have an impact on PHB accumulation in species of *Cupriavidus*. Bioproduction modeling suggests mutants of these genes may be less sensitive to dependence on nitrogen limitation and possibly other metabolic stresses than the wildtype organism to initiate PHB accumulation. Simulating PHB accumulation in an optimized, single-stage continuous reactor suggests these mutants may enable PHB production increases of 24% over the wildtype parent strain.

5 | METHODS

5.1 | Strains, medium, growth conditions

C. basilensis 4G11 (Ray et al., 2015) and previously generated RB-TnSeq library generated for this organism (Price et al., 2018) were

both maintained in R2A complex medium for general culture maintenance and storage. A similar library was unable to be constructed and adequately verified for use in the well-studied closely related species *C. necator*. The genomes of the two organisms are largely homologous (Supporting Information: Figure S1), and importantly the genomic *pha* locus was found to be highly homologous. We also were able to confirm that the two organisms make PHB with similar productivities and to similar final intracellular PHB wt%. For these reasons, the authors concluded that *C. basilensis* 4G11 was a suitable organism with which to conduct this study, and that any findings may transfer to *C. necator* and other closely related PHB-producing strains. Experiments were performed in defined DM9 medium (Wei et al., 2011) containing 2 g/L sodium acetate as the sole source of carbon and 1 g/L NH_4Cl as the sole source of nitrogen, unless otherwise noted. Cultures containing the *C. basilensis* 4G11 RB-TnSeq library (Price et al., 2018) were grown in medium containing 100 μg/mL kanamycin sulfate (Millipore Sigma part number 60615-5G). Cultures were grown and incubated at 30°C shaking at 250 rpm in Ultrayield flasks. Cultures containing *C. basilensis* 4G11 RB-TnSeq library were carried out in 2.5 L containing 1 L of culture volume. Experiments measuring PHB productivity were carried out in 250 mL ultrayield flasks containing 60 mL of culture volume. Oxygen saturation was verified in all growing conditions using a Fisherbrand Traceable Dissolved Oxygen Pen (part number 15-078-199). Cultures incubated in nitrogen-free medium were first grown for 24 h in replete DM9 medium containing 1 g/L NH_4Cl, after which cells were washed three times in DM9 containing 0 g/L NH_4Cl and resuspended in the same medium. These cultures were then incubated an additional 24 h to allow for PHB accumulation.

5.2 | Culturing in balanced growth conditions to suppress PHB production

It was found that frequent subcultures, maintaining an elevated growth rate, was able to suppress PHB accumulation in *C. basilensis* 4G11 (Supporting Information: Figure S2). This procedure was carried out by culturing cells in fresh medium and incubating for four to five generations before passaging the cells. This process was repeated with the culture OD_{600} value being kept perpetually below a value of 0.1, which we found to be the OD at which bulk PHB accumulation begins in our growing conditions (data not shown). This protocol was used to prepare RB-TnSeq library cells for subsequent screening, and to measure PHB productivity of subsequently generated markerless deletion mutant strains.

5.3 | Culturing in unbalanced growth conditions to maximize PHB production

Cells were inoculated into replete DM9 medium and incubated for 24 h at 30°C shaking at 250 rpm, yielding stationary phase culture. Cells were then washed three times with DM9 medium in which the NH_4Cl had been omitted (N-free DM9 medium). Each wash used

45 mL of N-free medium and was done by centrifuging the cells at 15,317g at 4°C for 10 min. Cells were then resuspended in nitrogen-free DM9 medium and incubated for an additional 24 h at 30°C, shaking at 250 rpm.

5.4 | Screening C. basilensis 4G11 RB-TnSeq libraries

C. basilensis 4G11 RB-TnSeq cells were grown as described above, to prepare replete-grown, low PHB cells to screen for putative constitutively producing PHB-producing mutants. The cells were then stained using BODIPY 493/503 dye (Invitrogen/ThermoFisher Scientific, part number D3922) to stain intracellular PHB (Kacmar et al., 2006). Stained cells were then analyzed and sorted on a Sony SH800 cell sorter, using the instrument's 488 nm excitation laser and FITC detection channel and performed in the instrument's "semi-purity" mode. Gates were constructed around the entire cell population based on forward scattering/side scattering bivariate plots (gate 1). Mutant populations were collected and analyzed from this gate to control for any bias the cell sorter may impart on strain enrichment outside of fluorescence, as done previously (Coradetti et al., 2018). Two other gates were also constructed representing (separately) the 5% most (gate 2) and 5% least (gate 3) fluorescent populations. To sort populations in which PHB accumulation had been suppressed (the "low" PHB population), >5 M cytometric events were collected which satisfied gate 1 + gate 2 (most fluorescent, highest PHB). In sorting populations that had been incubated in nitrogen-free medium (the "high PHB" population), >5 M cytometric events were collected which satisfied gate 1 + gate 2 (most fluorescent, highest PHB) and, separately, >5 M cytometric events which satisfied gate 1 + gate 3 (least fluorescent, lowest PHB). Cell fractions were sorted into 10 mL of DM9 medium containing 100 μg/mL kanamycin sulfate, transferred to 50 mL total volume of culture, and grown until early log phase. Fifty milliliter of this culture was collected and centrifuged at 15,317g at 4°C for 10 min. Supernatant was decanted and cells were transferred to a 1.5 mL Axygen 1.5 mL microtube (Axygen part number MCT-150-C). The cells were then centrifuged at 21,130g for 2 min at room temperature in a benchtop microcentrifuge (model number 5424; Eppendorf). The supernatant was decanted by aspiration and the cells were resuspended in 300 μL of a buffer consisting of 20 mM Tris- HCl (Fisher BioReagent part number BP2475-500), 2 mM sodium EDTA (Millipore Sigma part number E5134-50G), 1.2% Triton X-100 (Millipore Sigma part number X100-5ML), herein referred to as buffer enzymatic lysis buffer. The cell suspension was then stored at −80°C until DNA extraction was performed.

5.5 | Productivity screening

Screening mutants was done by growing cells as described previously. For replete-grown, PHB-suppressed cultures, samples

were collected and analyzed at the end of the fourth, fifth, and sixth subcultures/passages. One milliliter sample were collected for PHB analysis, centrifuged at 21,130g for 2 min at room temperature in an Eppendorf Centrifuge 5424, and dried overnight at 90°C. Dried pellets were then stored at −20°C. Pellets were processed similar to methods described previously (Tyo et al., 2009); 500 μL of concentrated H_2SO_4 (Millipore Sigma, part number 339,741) was added to the pellets and the mixture was heated at 90°C for 30 min in a stationary dry bath, vortexing briefly every 10 min. The samples were then allowed to cool at room temperature for 30 min, after which 500 μL of 5 mM H_2SO_4 was added and the mixture was vortexed thoroughly. One milliliter samples were also collected for analysis of supernatant acetate before and after each subculture, to assess the amount of acetate consumed. These samples were also centrifuged at 21,130g for 2 min at room temperature in an Eppendorf Centrifuge 5424, filtered through a 0.2 μm poly(vinylidene fluoride) syringe filter (Pall, part number 4406), and stored at −20°C until analysis. Digested samples for PHB analysis as well as filtered supernatants for acetate analysis were analyzed using a Shimadzu Prominence HPLC system equipped with a Biorad HPX 87H chromatography column (part number 1,250,140; Bio-rad Laboratories Inc.) and a diode array detector for UV detection. Both acetate and crotonic acid (the product of the above-mentioned PHB acid digestion) were analyzed at 206 nm. Cell dry weight enumerations were done by passing 45 mL of culture over a predried and pre-weighed 0.22 μm filter followed by two successive washes of 5 mL of milli-Q water. The filters were then dried overnight, allowed to cool to room temperature for 1 h and weighed again.

5.6 | Promoter alignment, candidate operator motif identification, and motif instance search

Previously, it was demonstrated that the acetyl CoA-synthetase (acs) gene is regulated by the CrbR transcription factor/response regulator in P. fluorescens (Sepulveda & Lupas, 2017). The putative LuxR-regulated acs homolog in the C. basilensis 4G11 genome was identified as the gene with the highest corresponding protein homology to acs from P. fluorescens: RR42_RS13380. 70 bp upstream of the RR42_RS13380 start codon was aligned to genomes from species in the genus Cupriavidus. From the set of aligning sequences, one representative sequence was taken from each species (11 species total, shown in Supporting Information: SI file "RS13380_up-stream. txt" and aligned sequences were inputted to the STREME motif/position weight matrix identification tool (Bailey, 2021). Motifs were identified using default parameters and settings. Among the candidate motifs identified, one contained a clear inverted repeat motif sequence to which LuxR family transcription factors in Gammaproteobacteria are known to bind (Novichkov et al., 2013). This motif was then used as input to the find individual motif occurances (FIMO) motif instance search tool (Grant et al., 2011) to

search for motif sites within the *C. basilensis* 4G11 genome. The FIMO tool was run using default parameters, yielding a list of individual candidate instances of the identified motif in the *C. basilensis* 4G11 genome.

5.7 | Whole proteome synteny mapping and TCS protein alignment of *C. basilensis* 4G11 and *C. necator* H16

Computing proteome synteny between *C. basilensis* 4G11 and *C. necator* H16 was done within KBase (Arkin et al., 2018), for which the public static narrative can be accessed at https://doi.org/10.25982/123676.7/1880128. Briefly, the genomes of both species (RefSeq accession NC_008313 for *C. necator* H16 and RefSeq accession NZ_CP010536 for *C. basilensis* 4G11) were uploaded and subsequently used to create a protein synteny plot (Supporting Information: Figure S1) using the "Compare Two Proteomes" app. Protein alignments between RR42_RS17055 and RR42_RS17060, and their respective homologs in the *C. necator* H16 genome (see Figure 3) were aligned using the "Pairwise Align" function in the Geneious Prime software (version 2022.2.2, https://www.geneious.com). Default values and parameters were used for this analysis.

5.8 | Batch growth, productivity modeling, and parameter fitting

We start by assuming that the data can be fit with a previously validated model (Islam Mozumder et al., 2015) and that O_2 is always saturated and can thus be neglected in our modeling. We used initial and final values of key concentrations from individual subculture of the ΔRR42_RS17055 and ΔRR42_RS17060 mutants from replete-grown subculture screening experiments (Figure 2, Supporting Information: Tables S3 and S4) to fit the model described below, assuming each subculture is a batch system. The model described temporal production of biomass and PHB as follows:

$$\frac{dc_X}{dt} = \mu_X c_X, \tag{1}$$

for biomass (c_X) and

$$\frac{dc_P}{dt} = \mu_P c_X, \tag{2}$$

for PHB (c_P). In both these equations, μ is the specific growth rate, given as

$$\mu_X = \mu_{max,X}\left(\frac{c_{Ac}}{K_{S,Ac} + c_{Ac} + \frac{c_{Ac}^2}{K_{I,Ac}}}\right)\left(\frac{c_N}{K_{S,N} + c_N + \frac{c_N^2}{K_{I,N}}}\right), \tag{3}$$

for biomass and

$$\mu_P = \mu_{max,P}\left(\frac{c_{Ac}}{K_{S,Ac} + c_{Ac} + \frac{c_{Ac}^2}{K_{I,Ac}}}\right)\left[1 - \left(\frac{f_{PHB}}{f_{PHB,max}}\right)^\beta\right]\left(\frac{K_{PIN}}{c_N + K_{PIN}}\right), \tag{4}$$

for PHB which both represent a maximum production rate mediated by terms which represent acetate uptake, ammonium chloride uptake, diversion of carbon to PHB as nitrogen becomes limiting, and a maximum sustainable amount of PHB per cell.

From these equations, the concentrations of acetate and nitrogen (as NH_4) are

$$\frac{dc_{Ac}}{dt} = \frac{-1}{Y_{\frac{X}{Ac}}}\mu_X c_X - \frac{1}{Y_{\frac{P}{Ac}}}\mu_P c_X, \tag{5}$$

and

$$\frac{dc_N}{dt} = \frac{-1}{Y_{\frac{X}{N}}}\mu_X c_X, \tag{6}$$

where $Y_{X/Ac}$, $Y_{P/Ac}$, and $Y_{X/N}$, are the yields of biomass (X) or PHB (P) on acetate (Ac) or ammonium (N).

5.9 | Parameter fitting

$K_{S,Ac}$, $K_{I,Ac}$, $K_{S,N}$, $K_{I,N}$, $f_{PHB,max}$, β, and $Y_{\frac{X}{N}}$ were taken from a previous study (Cestellos-Blanco et al., 2021).

Initial and final concentrations of acetate, cells, PHB, and nitrogen (as NH_3) were used to fit remaining parameters $\mu_{max,X}$, $\mu_{max,P}$, $Y_{\frac{X}{Ac}}$, $Y_{\frac{P}{Ac}}$, K_{PIN}, and $K_{S,N}$. Global parameter fitting over each of three batch runs (subcultures 4, 5, and 6) was performed simultaneously. Iterative parameter fitting was run to minimize the following error function using the generalized reduced gradient nonlinear solver function in Microsoft Excel, where c_{AC}, c_X, and c_{PHB} represent the concentration of sodium acetate, cell biomass, and PHB, respectively.

$$e = \sum_{j=Ac,X,PHB}\left[\frac{1}{c_j^{exp}}\sum_{i=4,5,6}\left(c_j^M - c_j^{exp,i}\right)^2\right]. \tag{7}$$

Specific growth rates were constrained to be <0.693/h consistent with that observed previously (Cestellos-Blanco et al., 2021).

5.10 | Continuous productivity modeling

All bioreactor models assume well-mixed gas and liquid phases that are exchanged at fixed liquid- and gas-phase dilution rates. In the liquid phase, we consider relevant dissolved constituents that can impact bioproduction (Abel et al., 2021): CO_2, dissolved O_2, bicarbonate anions (HCO_3^-), carbonate anions (CO_3^{2-}), protons (H^+), hydroxide anions (OH^-),

sodium cations (Na^+), chloride anions (Cl^-), acetate anions ($H_3C_2O_2^-$), acetic acid ($H_3C_2O_2H$), ammonia (NH_3), ammonium cations (NH_4^+), microbes (X), and PHB (monomer: $C_4H_6O_2$).

We consider both a single reactor system and a two-reactor system in which the reactors are connected in series. Equation development for the single reactor is equivalent to that of the first reactor in the two-reactor system. In all following equations, the subscript "n" refers to the reactor (n has a value either of 1 or 2), and the subscript "i" refers to a given species. The reactors are well-mixed and open such that they satisfy mass conservation, given generally for the liquid phase as:

$$\frac{dc_{n,i}}{dt} = R_{X,n,i} + R_{A-B,n,i} + R_{LF,n,i} + R_{G-L,n,i} + R_{pH,n,i}, \tag{8}$$

and for the gas phase as:

$$\frac{dp_{n,i}}{dt} = RT(R_{GF,n,i} - V_{LG,n}R_{G-L,n,i}), \tag{9}$$

where $c_{n,i}$ is the concentration; $p_{n,i}$ is the partial pressure; $R_{n,i}$ is the net volumetric rate of formation and consumption due to microbial growth (X), acid/base reactions (A–B), liquid or gas flow (LF/GF), gas/liquid mass transfer (G–L), and pH control (pH) for species i in reactor n; R is the gas constant; T is the operating temperature; and $V_{LG,n}$ is the ratio of liquid to gas volume in reactor n (which we assume to be equal to 2 in all cases).

5.11 | Microbial growth and PHB generation

Microbial growth and PHB generation occur in the well-mixed liquid phase and are responsible for the production of more cells and PHB, and the consumption or production of several chemical species. These reactions are compiled in $R_{X,n,i}$. Following Kachrimanidou et al. (2021); Pavan et al. (2019),

$$\begin{aligned} R_{X,n,X} &= \mu_{X,n}c_{n,X}, \\ R_{X,n,PHB} &= \mu_{PHB,n}c_{n,X}, \\ R_{X,n,i} &= \alpha_{X,i}\mu_{X,n}c_{n,X} + \alpha_{PHB,i}\mu_{PHB,n}c_{n,X}, \end{aligned} \tag{10}$$

where μ_X and μ_{PHB} are the specific growth rate of cells and the specific accumulation rate of PHB, and α_X and α_{PHB} are stoichiometric coefficients relating biomass growth and PHB accumulation to the consumption or production of other species, as defined below. We set $\alpha < 0$ if the species is consumed in the reaction. Growth kinetics are described with the inhibition-modified Monod (Andrews-Haldane) model:

$$\mu_{X,n} = \mu_{max,X,n}\left(\frac{c_{n,Ac}}{c_{n,Ac} + K_{S,Ac} + \frac{c_{n,Ac}^2}{K_{I,Ac}}}\right)\left(\frac{c_{n,O_2}}{K_{S,O_2} + c_{n,O_2}}\right)$$
$$\left(\frac{c_{n,NH_4}}{c_{n,NH_4} + K_{S,N} + \frac{c_{n,NH_4}^2}{K_{I,N}}}\right), \tag{11}$$

where $\mu_{max,X}$ is the maximum specific growth rate, and $K_{S,i}$ and $K_{I,i}$ are the half-saturation coefficient and inhibition coefficient for species i, respectively. We modify Pavan et al. (2019) to describe PHB accumulation:

$$\mu_{PHB,n} = \mu_{max,PHB,n}\left(\frac{c_{n,Ac}}{c_{n,Ac} + K_{S,Ac} + \frac{c_{n,Ac}^2}{K_{I,Ac}}}\right)\left(\frac{c_{n,O_2}}{K_{P,O_2} + c_{n,O_2}}\right)$$
$$\left[1 - \left(\frac{f_{n,PHB}}{f_{PHB,max}}\right)^\beta\right]\left(\frac{K_{PIN}}{c_{n,NH_4} + K_{PIN}}\right), \tag{12}$$

where $f_{PHB,(max)}$ is the (maximum) PHB-to-biomass ratio and K_{PIN} is the PHB inhibition coefficient for nitrogen.
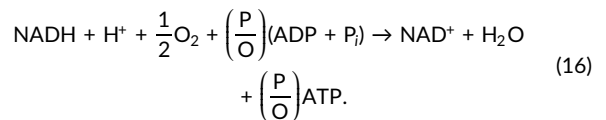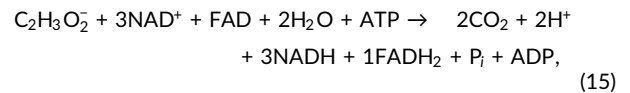
5.12 | Biomass and PHB yield on acetate

To determine experimental yields of biomass and PHB on acetate, we first calculated the theoretical yields following the stoichiometric and energetic approach we developed previously (Bellini et al., 2022). To determine the theoretical yield of biomass on acetate ($Y'^{,theo}_{X/Ac}$ fowing our previou), we follow the stoichiometry and energetics of acetate assimilation and oxidation. Acetate is first activated to acetyl-CoA via:

$$\begin{aligned} C_2H_3O_2^- + 2ATP + HSCoA + H^+ &\rightarrow C_2H_3OSCoA \\ &+ 2(ADP + Pi) + H_2O. \end{aligned} \tag{13}$$
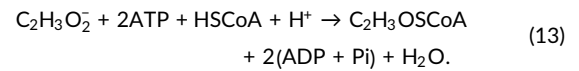
We modify the equation for biomass production from acetyl-CoA developed by Fast and Papoutsakis (Fast & Papoutsakis, 2012):

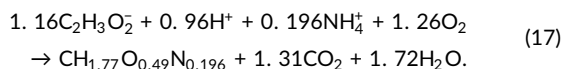$$0.5C_2H_3OSCoA + 4ATP + \frac{\Delta\gamma}{2}NADH \rightarrow CH_{1.77}O_{0.49}N_{0.196}, \tag{14}$$
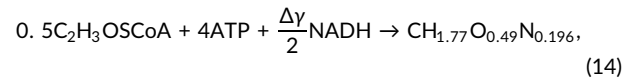
where $\Delta\gamma$ is the difference in the degree of reduction between acetyl-CoA ($\gamma = 4$) and biomass ($\gamma = 4.2$). We note that this equation, as written, is neither atomically nor charge balanced, so it should be taken to only represent the energy carrier demand of biomass formation. The required energy for acetate activation and acetyl-CoA conversion to biomass is provided by the catabolic reactions of the TCA cycle and by oxidative phosphorylation:

$$\begin{aligned} C_2H_3O_2^- + 3NAD^+ + FAD + 2H_2O + ATP &\rightarrow 2CO_2 + 2H^+ \\ &+ 3NADH + 1FADH_2 + P_i + ADP, \end{aligned} \tag{15}$$

$$\begin{aligned} NADH + H^+ + \frac{1}{2}O_2 + \left(\frac{P}{O}\right)(ADP + P_i) &\rightarrow NAD^+ + H_2O \\ &+ \left(\frac{P}{O}\right)ATP. \end{aligned} \tag{16}$$

Note that Equation (13) includes acetate activation to acetyl-CoA before its oxidation in the TCA cycle. We use a P/O ratio of

2.5 for NADH and 1.5 for FADH$_2$ following our previous report (Bellini et al., 2022). Combining these equations, and including NH$_4^+$ consumption to balance the nitrogen content of biomass, we obtain:

$$1.16C_2H_3O_2^- + 0.96H^+ + 0.196NH_4^+ + 1.26O_2 \\ \rightarrow CH_{1.77}O_{0.49}N_{0.196} + 1.31CO_2 + 1.72H_2O. \quad (17)$$
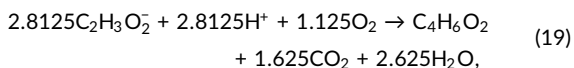
Hence, we use a theoretical molar yield of biomass on acetate of ~0.865 mol/mol (~0.36 g/g).

We use the same approach to calculate the molar yield of PHB on acetate but substitute the biomass-forming equation with the PHB-forming equation, which is given by:

$$2C_2H_3OSCoA + NADH + H^+ \rightarrow C_4H_6O_2 + 2HSCoA \\ + NAD^+. \quad (18)$$
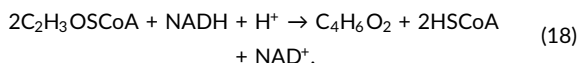
The overall stoichiometry is:

$$2.8125C_2H_3O_2^- + 2.8125H^+ + 1.125O_2 \rightarrow C_4H_6O_2 \\ + 1.625CO_2 + 2.625H_2O, \quad (19)$$

corresponding to a theoretical molar yield of PHB on acetate of ~0.356 mol/mol (~0.51 g/g).

To fit experimental yields of biomass and PHB on acetate, we defined a fractional value, θ_Y, as:

$$\theta_Y = \frac{Y_{X/Ac}^{exp}}{Y_{X/Ac}^{theo}} = \frac{Y_{PHB/Ac}^{exp}}{Y_{PHB/Ac}^{theo}}. \quad (20)$$

We assume these two ratios are equal on the basis that the metabolic processes producing PHB and cell biomass utilize the same source of carbon (acetate), and the same energy substrate-producing pathways (TCA cycle, oxidative phosphorylation). The production efficiencies of biomass and PHB should thus be nearly equivalent relative to their pathway-constrained maxima.

Hence, in our model, we calculate $\alpha_{X,n,i}$ and $\alpha_{PHB,n,i}$ according to:

$$\begin{aligned} \alpha_{X,Ac} &= \frac{1}{\theta_Y Y_{X/Ac}^{theo}}, \\ \alpha_{X,NH_4} &= 0.196, \\ \alpha_{X,H} &= \alpha_{X,Ac} - \alpha_{X,NH_4}, \\ \alpha_{X,O_2} &= \frac{1}{2}(0.49 + 2\alpha_{X,CO_2} + \alpha_{X,H_2O} - 2\alpha_{X,Ac}), \\ \alpha_{X,CO_2} &= 2\alpha_{X,Ac} - 1, \\ \alpha_{X,H_2O} &= \frac{1}{2}(4\alpha_{X,Ac} + 3\alpha_{X,NH_4} - 1.77), \end{aligned} \quad (21)$$

and

$$\begin{aligned} \alpha_{PHB,Ac} &= \frac{1}{\theta_Y Y_{PHB/Ac}^{theo}}, \\ \alpha_{PHB,NH_4} &= 0, \\ \alpha_{PHB,H} &= \alpha_{PHB,Ac} \\ \alpha_{PHB,O_2} &= 2\alpha_{PHB,Ac}-4.5, \\ \alpha_{PHB,CO_2} &= 2\alpha_{PHB,Ac}-4, \\ \alpha_{PHB,H_2O} &= 2\alpha_{PHB,Ac}-3. \end{aligned} \quad (22)$$

5.13 | Growth rate dependence on ph and salinity

We modify our previously developed model to describe the effects of pH and salinity on microbial growth (Bellini et al., 2022):

$$\begin{aligned} \mu_{max,X,n} &= \mu_{opt,X}\rho(pH_n)\nu(c_{n,Na}), \\ \mu_{max,PHB,n} &= \mu_{opt,PHB}\rho(pH_n)\nu(c_{n,Na}), \end{aligned} \quad (23)$$

where $\mu_{opt,X}$ and $\mu_{opt,PHB}$ are the specific growth and PHB accumulation rates at optimal conditions, and $\rho(pH)$ and $\nu(c_{Na})$ are functions describing the impacts of pH and Na$^+$ concentration on the growth rate. Following our previous work (Bellini et al., 2022), we write $\rho(pH)$ as:

$$\rho(pH_n) = \begin{cases} 0 & pH_n < pH_{min} \\ f(pH_n) & pH_{min} \le pH_n \le pH_{max}. \\ 0 & pH_n > pH_{max} \end{cases} \quad (24)$$

Here, $pH_{min/max}$ is the range of pH over which microbial growth is observed, and the function $f(pH_n)$ is:

$$f(pH_n) = \frac{(pH_n - pH_{min})(pH_n - pH_{max})}{(pH_n - pH_{min})(pH_n - pH_{max}) - (pH_n - pH_{opt})^2}, \quad (25)$$

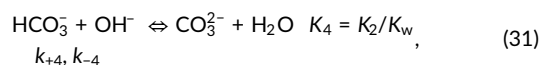where pH_{opt} is the optimal pH for growth. Similarly, we define $\nu(c_{Na})$ as:
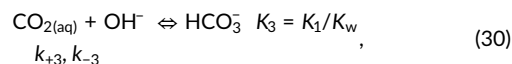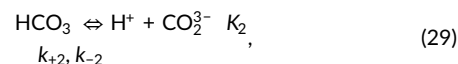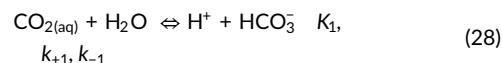
$$\nu(c_{n,Na}) = \begin{cases} 1 & c_{n,Na} < c_{Na,min} \\ f(c_{n,Na}) & c_{Na,min} < c_{n,Na} < c_{Na,max}, \\ 0 & c_{n,Na} > c_{Na,max} \end{cases} \quad (26)$$

where $c_{Na,min/max}$ is the range of Na$^+$ concentration over which growth is impacted, and the function $f(c_{Na})$ is given by:
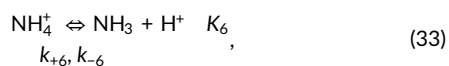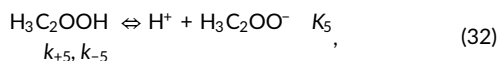
$$f(c_{n,Na}) = 1 - \frac{c_{n,Na}}{c_{Na,max} - c_{Na,min}}. \quad (27)$$

5.14 | Acid/base reactions

The acid/base carbon dioxide/bicarbonate/carbonate, acetate/acetic acid, ammonia/ammonium, and water dissociation reactions shown below occur in the liquid phase and are treated as kinetic expressions without assuming equilibrium:

$$\begin{aligned} CO_{2(aq)} + H_2O &\Leftrightarrow H^+ + HCO_3^- \quad K_1, \\ &k_{+1}, k_{-1} \end{aligned} \quad (28)$$

$$\begin{aligned} HCO_3 &\Leftrightarrow H^+ + CO_2^{3-} \quad K_2, \\ &k_{+2}, k_{-2} \end{aligned} \quad (29)$$

$$\begin{aligned} CO_{2(aq)} + OH^- &\Leftrightarrow HCO_3^- \quad K_3 = K_1/K_w, \\ &k_{+3}, k_{-3} \end{aligned} \quad (30)$$

$$\begin{aligned} HCO_3^- + OH^- &\Leftrightarrow CO_3^{2-} + H_2O \quad K_4 = K_2/K_w, \\ &k_{+4}, k_{-4} \end{aligned} \quad (31)$$

$$H_3C_2OOH \Leftrightarrow H^+ + H_3C_2OO^- \quad K_5, \atop k_{+5}, k_{-5} \tag{32}$$

$$NH_4^+ \Leftrightarrow NH_3 + H^+ \quad K_6, \atop k_{+6}, k_{-6} \tag{33}$$

$$H_2O \Leftrightarrow H^+ + OH^- \quad K_w, \atop k_{+w}, k_{-w} \tag{34}$$

where k_{+k} and k_{-k} are the forward and reverse rate constants, respectively, and K_k is the equilibrium constant for the nth reaction. For acetic acid and water, we calculate K_k from the van't Hoff equation using the change of entropy, ΔS_k, and the heat of reaction, ΔH_k, given by:

$$K_k = \exp\left(\frac{\Delta S_k}{R}\right)\exp\left(\frac{-\Delta H_k}{RT}\right). \tag{35}$$

For CO_2/HCO_3^- and HCO_3^-/CO_3^{2-} equilibria, we calculate K_k using the empirical relationships compiled by W. G. Mook that account for salinity-induced impacts on the equilibrium constant (Choi et al., 2020):

$$pK_1 = \frac{3670.7}{T} - 62.008 + 9.7944\ln(T) - 0.0118S + 0.000116S^2, \tag{36}$$

$$pK_2 = \frac{1394.7}{T} + 4.777 - 0.0184S + 0.000118S^2, \tag{37}$$

where S is the medium salinity (in units g/kg water).

Source and sink terms resulting from these reactions are compiled in $R_{A-B,n,i}$, written as:

$$R_{A-B,n,i} = \sum_i v_i\left(k_{+k}\prod_{v_i<0} c_{n,i} - k_{-k}\prod_{v_i>0} c_{n,i}\right), \tag{38}$$

where v_i is the stoichiometric coefficient of species i for the kth reaction and reverse rate constants (k_{-k}) are calculated from:

$$k_{-k} = \frac{k_{+k}}{K_k}. \tag{39}$$

5.15 | Liquid and gas flow

Liquid media flows into and out of the well-mixed liquid phase at a constant dilution date ($D_{liq,n}$). In the first reactor (or lone reactor in the single-reactor system), this results in a feed term written as:

$$R_{LF,1,i} = D_{liq,1}(c_{f,1,i} - c_{1,i}), \tag{40}$$

where $c_{f,1,i}$ is the concentration of species i in the feed stream to reactor 1. In the two-reactor system, we account for two liquid phase flows. First, the effluent from reactor 1 is fed to reactor 2 directly with no processing. Second, an additional feed stream is optionally applied to supply, for example, additional N-free substrate that can be converted to PHB. On a volumetric basis, then, the total liquid flow rate into the second reactor is the sum of the flow rate out of the first reactor and the additional feed stream flow rate. Hence, the liquid feed term for the second reactor is written as:

$$R_{LF,2,i} = D_{liq,1}V_{12}(c_{1,i} - c_{f,2,i}) + D_{liq,2}(c_{f,2,i} - c_{2,i}), \tag{41}$$

where V_{12} is the volumetric ratio of reactor 1 to reactor 2 and $c_{f,2,i}$ is the concentration of species i in the optional additional feed stream to reactor 2. Note that when the additional feed stream is not applied, $D_{liq,1}V_{12} = D_{liq,2}$ and $c_{f,2,i} = 0$ such that the right-hand side of Equation (34) collapses to $D_{liq,2}(c_{1,i} - c_{2,i})$ as expected.

For the gas phase(s), we define a feed term according to:

$$R_{GF,n,i} = \frac{D_{gas,n}}{RT}(p_{f,n,i} - p_{n,i}), \tag{42}$$

where $D_{gas,n}$ is the gas-phase dilution rate in reactor n.

5.16 | Gas–liquid mass transfer

Gas fed to the reactors results in mass transfer to the liquid phase according to:

$$R_{G-L,n,i} = k_La_i(\beta_{n,i}p_{n,i} - c_{n,i}) \tag{43}$$

where k_La_i us the volumetric mass-transfer coefficient on the liquid side of the gas/liquid interface and $\beta_{n,i}$ is the Bunsen solubility coefficient. We assume $k_La_{O_2}$ is 300/h following our previous analysis (Atlić et al., 2011), which represents an intermediate value of the range observed in standard bioreactors (Kim et al., 1994; Vlaeminck et al., 2022). To calculate $k_La_{CO_2}$, we use:

$$k_La_{CO_2} = \sqrt{\frac{D_{CO_2}}{D_{O_2}}}k_La_{O_2}, \tag{44}$$

where D_{O_2} and D_{CO_2} are the diffusivities of O_2 and CO_2 following Meraz et al. (2020) to account for the differences in the mass transfer coefficient (Franz et al., 2011).

We calculate the equilibrium solubility of O_2 and CO_2 according to the empirical relationship for the Bunsen solubility coefficient (β):

$$\ln\beta = A_1 + A_2\left(\frac{100}{T}\right) + A_3\ln\left(\frac{T}{100}\right) + S\left[B_1 + B_2\left(\frac{T}{100}\right) + B_3\left(\frac{T}{100}\right)^2\right], \tag{45}$$

where A and B are fitting parameters and S is the medium salinity (in units g/kg water).

5.17 | pH control

A feedback control loop is included in the reactor to maintain an optimal pH for microbial growth by adding 1 M sodium hydroxide solution

when appropriate. The manipulated flow rate variable (units/h) is defined as:

$$r_{M,n} = 0 + K_C\left(E_n + \frac{1}{\tau}\int E_n dt\right), \tag{46}$$

where K_C is the controller gain, E is the error, and τ is the controller reset time. The error (E) is defined according to:

$$E_n = pH^{set} - pH_n, \tag{47}$$

where pH^{set} is equivalent to pH_{opt}. The resulting pH control flow is given by:

$$R_{pH,n,i} = r_{M,n}c_{pH,,i,} \tag{48}$$

where $c_{pH,i}$ is 1M for OH^- and Na^+.

5.18 | Model analysis

In the single-reactor system, PHB productivity was calculated using:

$$P_{1,PHB} = D_{liq,1}c_{1,PHB}. \tag{49}$$

In the two-reactor system, we calculated the overall productivity by normalizing to the combined volume of the reactors, resulting in:

$$P_{2,PHB} = \frac{D_{liq,2}c_{2,PHB}}{1 + V_{12}}. \tag{50}$$

5.19 | Model implementation

All equations were solved using the MUMPS general solver in COMSOL Multiphysics 5.4. Model parameters are listed in Supporting Information: Table S2.

AUTHOR CONTRIBUTIONS

Kyle Sander: Conceptualization, data curation, formal analysis, investigation, methodology, project administration, validation, visualization, writing—original draft, writing—review and editing. **Anthony J. Abel**: Formal analysis, methodology, visualization, writing—original draft, writing—review and editing. **Skyler Friedline**: Formal analysis, investigation, methodology, validation, visualization, writing—review and editing. **William Sharpless**: Investigation, methodology, writing—review and editing. **Jeffrey Skerker**: Conceptualization, data curation, project administration, validation. **Adam Deutschbauer**: Resources, validation. **Douglas S. Clark**: Methodology, project administration, validation, writing—review and editing, project administration, funding acquisition. **Adam P. Arkin**: Conceptualization, investigation, formal analysis, methodology, project administration, writing—review and editing, funding acquisition.

CONFLICT OF INTEREST STATEMENT

The authors declare no conflict of interest.

DATA AVAILABILITY STATEMENT

All plasmids used in this study are available through Addgene (https://www.addgene.org/, see Supporting Information: Table S5 for deposit numbers). All strains used in this study (Supporting Information: Table S6) are available upon request. Primers used in this study are listed in Supporting Information: Table S7. The static narrative (10.25982/123676.7/1880128) for generating Supporting Information: Figure S1 is available at https://doi.org/10.25982/123676.7/1880128. The data that support the findings of this study are openly available in KBase Narrative—Comparing Proteomes of Cupriavidus basilen at https://www.osti.gov/biblio/1880128, reference number https://doi.org/10.25982/123676.7/1880128.

ORCID

Kyle Sander http://orcid.org/0000-0002-5944-7822

REFERENCES

Abel, A. J., Adams, J. D., & Clark, D. S. (2022). A comparative life cycle analysis of electromicrobial production systems. *Energy & Environmental Science*, *15*, 3062–3085. https://doi.org/10.1101/2021.07.01.450744

Ahn, W. S., Park, S. J., & Lee, S. Y. (2000). Production of Poly(3-hydroxybutyrate) by fed-batch culture of recombinant *Escherichia coli* with a highly concentrated whey solution. *Applied and Environmental Microbiology*, *66*, 3624–3627.

Al Rowaihi, I. S., Paillier, A., Rasul, S., Karan, R., Grötzinger, S. W., Takanabe, K., & Eppinger, J. (2018). Poly(3-hydroxybutyrate) production in an integrated electromicrobial setup: Investigation under stress-inducing conditions. *PLoS ONE*, *13*, e0196079.

Alsiyabi, A., Brown, B., Immethun, C., Long, D., Wilkins, M., & Saha, R. (2021). Synergistic experimental and computational approach identifies novel strategies for polyhydroxybutyrate overproduction. *Metabolic Engineering*, *68*, 1–13.

Arkin, A. P., Cottingham, R. W., Henry, C. S., Harris, N. L., Stevens, R. L., Maslov, S., Dehal, P., Ware, D., Perez, F., Canon, S., Sneddon, M. W., Henderson, M. L., Riehl, W. J., Murphy-Olson, D., Chan, S. Y., Kamimura, R. T., Kumari, S., Drake, M. M., Brettin, T. S., ... Yu, D.

(2018). KBase: The United States department of energy systems biology knowledgebase. *Nature Biotechnology*, 36, 566–569.

Atlić, A., Koller, M., Scherzer, D., Kutschera, C., Grillo-Fernandes, E., Horvat, P., Chiellini, E., & Braunegg, G. (2011). Continuous production of poly([R]−3-hydroxybutyrate) by *Cupriavidus necator* in a multistage bioreactor cascade. *Applied Microbiology and Biotechnology*, 91, 295–304.

Bailey, M. J., & Tähtiharju, J. (2003). Efficient cellulase production by *Trichoderma reesei* in continuous cultivation on lactose medium with a computer-controlled feeding strategy. *Applied Microbiology and Biotechnology*, 62, 156–162.

Bailey, T. L. (2021). STREME: Accurate and versatile sequence motif discovery. *Bioinformatics*, 37, 2834–2840.

Barrett, C. F., & Parker, M. A. (2006). Coexistence of *Burkholderia*, *Cupriavidus*, and *Rhizobium* sp. Nodule Bacteria on two Mimosa spp. in Costa Rica. *Applied and Environmental Microbiology*, 72, 1198–1206.

Bellini, S., Tommasi, T., & Fino, D. (2022). Poly(3-hydroxybutyrate) biosynthesis by *Cupriavidus necator*: A review on waste substrates utilization for a circular economy approach. *Bioresource Technology Reports*, 17, 100985.

Berliner, A. J., Hilzinger, J. M., Abel, A. J., McNulty, M. J., Makrygiorgos, G., Averesch, N. J. H., Sen Gupta, S., Benvenuti, A., Caddell, D. F., Cestellos-Blanco, S., Doloman, A., Friedline, S., Ho, D., Gu, W., Hill, A., Kusuma, P., Lipsky, I., Mirkovic, M., Luis Meraz, J., ... Arkin, A. P. (2021). Towards a biomanufactory on mars. *Frontiers in Astronomy and Space Sciences*, 8, 120.

Cai, S., Cai, L., Zhao, D., Liu, G., Han, J., Zhou, J., & Xiang, H. (2015). A novel DNA-binding protein, PhaR, plays a central role in the regulation of polyhydroxyalkanoate accumulation and granule formation in the Haloarchaeon *Haloferax mediterranei*. *Applied and Environmental Microbiology*, 81, 373–385.

Castañeda, M., Guzmán, J., Moreno, S., & Espín, G. (2000). The GacS sensor kinase regulates alginate and poly-β-hydroxybutyrate production in *Azotobacter vinelandii*. *Journal of Bacteriology*, 182, 2624–2628.

Cavalheiro, J. M. B. T., de Almeida, M. C. M. D., Grandfils, C., & da Fonseca, M. M. R. (2009). Poly(3-hydroxybutyrate) production by *Cupriavidus necator* using waste glycerol. *Process Biochemistry*, 44, 509–515.

Cestellos-Blanco, S., Friedline, S., Sander, K. B., Abel, A. J., Kim, J. M., Clark, D. S., Arkin, A. P., & Yang, P. (2021). Production of PHB from CO_2-derived acetate with minimal processing assessed for space biomanufacturing. *Frontiers in Microbiology*, 12, 2126.

Choi, J., & Lee, S. Y. (1999). Factors affecting the economics of polyhydroxyalkanoate production by bacterial fermentation. *Applied Microbiology and Biotechnology*, 51, 13–21.

Choi, J., Lee, S. Y., & Han, K. (1998). Cloning of the *Alcaligenes latus* polyhydroxyalkanoate biosynthesis genes and use of these genes for enhanced production of poly(3-hydroxybutyrate) in *Escherichia coli*. *Applied and Environmental Microbiology*, 64, 4897–4903.

Choi, S. Y., Rhie, M. N., Kim, H. T., Joo, J. C., Cho, I. J., Son, J., Jo, S. Y., Sohn, Y. J., Baritugo, K. A., Pyo, J., Lee, Y., Lee, S. Y., & Park, S. J. (2020). Metabolic engineering for the synthesis of polyesters: A 100-year journey from polyhydroxyalkanoates to non-natural microbial polyesters. *Metabolic Engineering*, 58, 47–81.

Coradetti, S. T., Pinel, D., Geiselman, G. M., Ito, M., Mondo, S. J., Reilly, M. C., Cheng, Y. F., Bauer, S., Grigoriev, I. V., Gladden, J. M., Simmons, B. A., Brem, R. B., Arkin, A. P., & Skerker, J. M. (2018). Functional genomics of lipid metabolism in the oleaginous yeast *Rhodosporidium toruloides*. *eLife*, 7, e32110.

Fast, A. G., & Papoutsakis, E. T. (2012). Stoichiometric and energetic analyses of non-photosynthetic CO2-fixation pathways to support synthetic biology strategies for production of fuels and chemicals. *Current Opinion in Chemical Engineering*, 1, 380–395.

Fisher, A. C., Kamga, M. H., Agarabi, C., Brorson, K., Lee, S. L., & Yoon, S. (2019). The current scientific and regulatory landscape in advancing integrated continuous biopharmaceutical manufacturing. *Trends in Biotechnology*, 37, 253–267.

Franz, A., Song, H.-S., Ramkrishna, D., & Kienle, A. (2011). Experimental and theoretical analysis of poly(β-hydroxybutyrate) formation and consumption in *Ralstonia eutropha*. *Biochemical Engineering Journal*, 55, 49–58.

Garg, R. P., Huang, J., Yindeeyoungyeon, W., Denny, T. P., & Schell, M. A. (2000). Multicomponent transcriptional regulation at the complex promoter of the Exopolysaccharide I biosynthetic operon of *Ralstonia solanacearum*. *Journal of Bacteriology*, 182, 6659–6666.

Grant, C. E., Bailey, T. L., & Noble, W. S. (2011). FIMO: Scanning for occurrences of a given motif. *Bioinformatics*, 27, 1017–1018.

Grousseau, E., Lu, J., Gorret, N., Guillouet, S. E., & Sinskey, A. J. (2014). Isopropanol production with engineered *Cupriavidus necator* as bioproduction platform. *Applied Microbiology and Biotechnology*, 98, 4277–4290.

Harrison, R. G., Todd, P. W., Rudge, S. R., & Petrides, D. P. (2015). Bioprocess design and economics. In R. G. Harrison, P. W. Todd, S. R. Rudge, & D. P. Petrides (Eds.), *Bioseparations science and engineering*. Oxford University Press. https://doi.org/10.1093/oso/9780195391817.003.0015

Hernandez-Eligio, A., Moreno, S., Castellanos, M., Castañeda, M., Nuñez, C., Muriel-Millan, L. F., & Espín, G. (2012). RsmA post-transcriptionally controls PhbR expression and polyhydroxybutyrate biosynthesis in *Azotobacter vinelandii*. *Microbiology*, 158, 1953–1963.

Horng, Y.-T., Chang, K. C., Chien, C. C., Wei, Y. H., Sun, Y. M., & Soo, P. C. (2010). Enhanced polyhydroxybutyrate (PHB) production via the coexpressed phaCAB and vgb genes controlled by arabinose PBAD promoter in *Escherichia coli*. *Letters in Applied Microbiology*, 50, 158–167.

Islam Mozumder, M. S., Garcia-Gonzalez, L, Wever, H. D., & Volcke, E. I. P. (2015). Poly(3-hydroxybutyrate) (PHB) production from CO_2: Model development and process optimization. *Biochemical Engineering Journal*, 98, 107–116.

Juengert, J. R., Borisova, M., Mayer, C., Wolz, C., Brigham, C. J., Sinskey, A. J., & Jendrossek, D. (2017). Absence of ppGpp leads to increased mobilization of intermediately accumulated poly(3-hydroxybutyrate) in *Ralstonia eutropha* H16. *Applied and Environmental Microbiology*, 83(13), e00755–17. https://doi.org/10.1128/AEM.00755-17

Juengert, J. R., Patterson, C., & Jendrossek, D. (2018). Poly(3-hydroxybutyrate) (PHB) polymerase PhaC1 and PHB depolymerase PhaZa1 of *Ralstonia eutropha* are phosphorylated in vivo. *Applied and Environmental Microbiology*, 84, e00604–e00618.

Kachrimanidou, V., Ioannidou, S. M., Ladakis, D., Papapostolou, H., Kopsahelis, N., Koutinas, A. A., & Kookos, I. K. (2021). Techno-economic evaluation and life-cycle assessment of poly(3-hydroxybutyrate) production within a biorefinery concept using sunflower-based biodiesel industry by-products. *Bioresource Technology*, 326, 124711.

Kacmar, J., Carlson, R., Balogh, S. J., & Srienc, F. (2006). Staining and quantification of poly-3-hydroxybutyrate in *Saccharomyces cerevisiae* and cupriavidus necator cell populations using automated flow cytometry. *Cytometry Part A*, 69A, 27–35.

Karstens, K., Zschiedrich, C. P., Bowien, B., Stülke, J., & Görke, B. (2014). Phosphotransferase protein EIIANtr interacts with SpoT, a key enzyme of the stringent response, in *Ralstonia eutropha* H16. *Microbiology*, 160, 711–722.

Kim, B. S., Lee, S. C., Lee, S. Y., Chang, H. N., Chang, Y. K., & Woo, S. I. (1994). Production of poly(3-hydroxybutyric acid) by fed-batch culture of *Alcaligenes eutrophus* with glucose concentration control. *Biotechnology and Bioengineering*, 43, 892–898.

Klamt, S., & Mahadevan, R. (2015). On the feasibility of growth-coupled product synthesis in microbial strains. *Metabolic Engineering*, *30*, 166–178.

Koller, M., & Braunegg, G. (2015). Potential and prospects of continuous polyhydroxyalkanoate (PHA) production. *Bioengineering*, *2*, 94–121.

Konstantinov, K. B., & Cooney, C. L. (2015). White paper on continuous bioprocessing. May 20–21, 2014 continuous manufacturing symposium. *Journal of Pharmaceutical Sciences*, *104*, 813–820.

Krauβe, D., Hunold, K., Kusian, B., Lenz, O., Stülke, J., Bowien, B., & Deutscher, J. (2009). Essential role of the hprK gene in *Ralstonia eutropha*. *Journal of Molecular Microbiology and Biotechnology*, *17*(3), 146–152.

Lee, S. Y., & Chang, H. N. (1993). High cell density cultivation of *Escherichia coli* W using sucrose as a carbon source. *Biotechnology Letters*, *15*, 971–974.

Lykidis, A., Pérez-Pantoja, D., Ledger, T., Mavromatis, K., Anderson, I. J., Ivanova, N. N., Hooper, S. D., Lapidus, A., Lucas, S., González, B., & Kyrpides, N. C. (2010). The complete multipartite genome sequence of cupriavidus necator JMP134, a versatile pollutant degrader. *PLoS ONE*, *5*, e9729.

Meraz, J. L., Dubrawski, K. L., El Abbadi, S. H., Choo, K.-H., & Criddle, C. S. (2020). Membrane and fluid contactors for safe and efficient methane delivery in methanotrophic bioreactors. *Journal of Environmental Engineering*, *146*, 03120006.

Mitra, R., Xu, T., Chen, G.-Q., Xiang, H., & Han, J. (2022). An updated overview on the regulatory circuits of polyhydroxyalkanoates synthesis. *Microbial Biotechnology*, *15*, 1446–1470.

Mori, Y., Ishikawa, S., Ohnishi, H., Shimatani, M., Morikawa, Y., Hayashi, K., Ohnishi, K., Kiba, A., Kai, K., & Hikichi, Y. (2018). Involvement of ralfuranones in the quorum sensing signalling pathway and virulence of *Ralstonia solanacearum* strain OE1-1. *Molecular Plant Pathology*, *19*, 454–463.

Napathorn, S. C., Visetkoop, S., Pinyakong, O., Okano, K., & Honda, K. (2021). Polyhydroxybutyrate (PHB) production using an arabinose-inducible expression system in comparison with cold shock inducible expression system in *Escherichia coli*. *Frontiers in Bioengineering and Biotechnology*, *9*, 661096. https://doi.org/10.3389/fbioe.2021.661096

Novichkov, P. S., Kazakov, A. E., Ravcheev, D. A., Leyn, S. A., Kovaleva, G. Y., Sutormin, R. A., Kazanov, M. D., Riehl, W., Arkin, A. P., Dubchak, I., & Rodionov, D. A. (2013). RegPrecise 3.0—A resource for genome-scale exploration of transcriptional regulation in bacteria. *BMC Genomics*, *14*, 745.

Olavarria, K., Pijman, Y. O., Cabrera, R., van Loosdrecht, M. C. M., & Wahl, S. A. (2022). Engineering an acetoacetyl-CoA reductase from *Cupriavidus necator* toward NADH preference under physiological conditions. *Scientific Reports*, *12*, 3757.

Olaya-Abril, A., Luque-Almagro, V. M., Manso, I., Gates, A. J., Moreno-Vivián, C., Richardson, D. J., & Roldán, M. D. (2018). Poly(3-hydroxybutyrate) hyperproduction by a global nitrogen regulator NtrB mutant strain of *Paracoccus denitrificans* PD1222. *FEMS Microbiology Letters*, *365*, fnx251.

Pavan, F. A., Junqueira, T. L., Watanabe, M. D. B., Bonomi, A., Quines, L. K., Schmidell, W., & de Aragao, G. M. F. (2019). Economic analysis of polyhydroxybutyrate production by *Cupriavidus necator* using different routes for product recovery. *Biochemical Engineering Journal*, *146*, 97–104.

Pötter, M., Müller, H., & Steinbüchel, A. (2005). Influence of homologous phasins (PhaP) on PHA accumulation and regulation of their expression by the transcriptional repressor PhaR in *Ralstonia eutropha* H16. *Microbiology*, *151*, 825–833.

Price, M., Lo, V., & Shao, W. (2021). *Fitness browser*. Retrieved December 2022 from https://fit.genomics.lbl.gov/

Price, M. N., Wetmore, K. M., Waters, R. J., Callaghan, M., Ray, J., Liu, H., Kuehl, J. V., Melnyk, R. A., Lamson, J. S., Suh, Y., Carlson, H. K., Esquivel, Z., Sadeeshkumar, H., Chakraborty, R., Zane, G. M.,

Rubin, B. E., Wall, J. D., Visel, A., Bristow, J., … Deutschbauer, A. M. (2018). Mutant phenotypes for thousands of bacterial genes of unknown function. *Nature*, *557*, 503–509.

Rajeev, L., Garber, M. E., & Mukhopadhyay, A. (2020). Tools to map target genes of bacterial two-component system response regulators. *Environmental Microbiology Reports*, *12*, 267–276.

Ray, J., Waters, R. J., Skerker, J. M., Kuehl, J. V., Price, M. N., Huang, J., Chakraborty, R., Arkin, A. P., & Deutschbauer, A. (2015). Complete genome sequence of *Cupriavidus basilensis* 4G11, isolated from the Oak Ridge Field Research Center Site. *Genome Announcements*, *3*(3), e00322–15. https://doi.org/10.1128/genomea.00322-15

Ryan, W. J., O'Leary, N. D., O'Mahony, M., & Dobson, A. D. W. (2013). GacS-dependent regulation of polyhydroxyalkanoate synthesis in *Pseudomonas putida* CA-3. *Applied and Environmental Microbiology*, *79*, 1795–1802.

Sacomboio, E. N. M., Kim, E. Y. S., Ruchaud Correa, H. L., Bonato, P., de Oliveira Pedrosa, F., de Souza, E. M., Chubatsu, L. S., & Müller-Santos, M. (2017). The transcriptional regulator NtrC controls glucose-6-phosphate dehydrogenase expression and polyhydroxy-butyrate synthesis through NADPH availability in *Herbaspirillum seropedicae*. *Scientific Reports*, *7*, 13546.

Schell, M. A. (2000). Control of virulence and pathogenicity genes of *Ralstonia solanacearum* by an elaborate sensory network. *Annual Review of Phytopathology*, *38*, 263–292.

Schmidt, M., Ienczak, J. L., Quines, L. K., Zanfonato, K., Schmidell, W., & de Aragão, G. M. F. (2016). Poly(3-hydroxybutyrate-co-3-hydroxyvalerate) production in a system with external cell recycle and limited nitrogen feeding during the production phase. *Biochemical Engineering Journal*, *112*, 130–135.

Sepulveda, E., & Lupas, A. N. (2017). Characterization of the CrbS/R two-component system in *Pseudomonas fluorescens* reveals a new set of genes under its control and a DNA motif required for CrbR-mediated transcriptional activation. *Frontiers in Microbiology*, *8*, 2287. https://doi.org/10.3389/fmicb.2017.02287

Shanks, R. M. Q., Caiazza, N. C., Hinsa, S. M., Toutain, C. M., & O'Toole, G. A. (2006). *Saccharomyces cerevisiae*-based molecular tool kit for manipulation of genes from gram-negative bacteria. *Applied and Environmental Microbiology*, *72*, 5027–5036.

Shi, Y. (2009). Serine/threonine phosphatases: Mechanism through structure. *Cell*, *139*, 468–484.

Tang, R., Peng, X., Weng, C., & Han, Y. (2022). The overexpression of phasin and regulator genes promoting the synthesis of polyhydroxy-ybutyrate in cupriavidus necator H16 under nonstress conditions. *Applied and Environmental Microbiology*, *88*, e01458–21.

Testa, R. L., Delpino, C., Estrada, V., & Diaz, M. S. (2022). Development of in silico strategies to photoautotrophically produce poly-β-hydroxybutyrate (PHB) by cyanobacteria. *Algal Research*, *62*, 102621.

Theodorou, E. C., Theodorou, M. C., & Kyriakidis, D. A. (2012). Involvement of the AtoSCDAEB regulon in the high molecular weight poly-(R)-3-hydroxybutyrate biosynthesis in phaCAB+ *Escherichia coli*. *Metabolic Engineering*, *14*, 354–365.

Tyo, K. E. J., Jin, Y. S., Espinoza, F. A., & Stephanopoulos, G. (2009). Identification of gene disruptions for increased poly-3-hydroxybutyrate accumulation in *Synechocystis* PCC 6803. *Biotechnology Progress*, *25*, 1236–1243.

Vadlja, D., Koller, M., Novak, M., Braunegg, G., & Horvat, P. (2016). Footprint area analysis of binary imaged *Cupriavidus necator* cells to study PHB production at balanced, transient, and limited growth conditions in a cascade process. *Applied Microbiology and Biotechnology*, *100*, 10065–10080.

Velázquez-Sánchez, C., Espín, G., Peña, C., & Segura, D. (2020). The modification of regulatory circuits involved in the control of polyhydroxyalkanoates metabolism to improve their production. *Frontiers in Bioengineering and Biotechnology*, *8*, 386. https://doi.org/10.3389/fbioe.2020.00386

Vlaeminck, E., Quataert, K., Uitterhaegen, E., De Winter, K., & Soetaert, W. K. (2022). Advanced PHB fermentation strategies with CO_2-derived organic acids. *Journal of Biotechnology*, *343*, 102–109.

Wang, F., & Lee, S. Y. (1997). Poly(3-hydroxybutyrate) production with high productivity and high polymer content by a fed-batch culture of alcaligenes latus under nitrogen limitation. *Applied and Environmental Microbiology*, *63*, 3703–3706.

Van Wegen, R. J., Ling, Y., & Middelberg, A. P. J. (1998). Industrial production of polyhydroxyalkanoates using *Escherichia coll*: An economic analysis. *Chemical Engineering Research and Design*, *76*, 417–426.

Wei, Y.-H., Chen, W. C., Huang, C. K., Wu, H. S., Sun, Y. M., Lo, C. W., & Janarthanan, O. M. (2011). Screening and evaluation of polyhydroxybutyrate-producing strains from indigenous isolate *Cupriavidus taiwanensis* strains. *International Journal of Molecular Sciences*, *12*, 252–265.

Yang, O., Qadan, M., & Ierapetritou, M. (2020). Economic analysis of batch and continuous biopharmaceutical antibody production: A review. *Journal of Pharmaceutical Innovation*, *15*, 182–200.

York, G. M., Stubbe, J., & Sinskey, A. J. (2002). The *Ralstonia eutropha* PhaR protein couples synthesis of the PhaP phasin to the presence of polyhydroxybutyrate in cells and promotes polyhydroxybutyrate production. *Journal of Bacteriology*, *184*, 59–66.

SUPPORTING INFORMATION

Additional supporting information can be found online in the Supporting Information section at the end of this article.